Phase-composition dependent domain responses in $(K_{0.5}Na_{0.5})NbO_3$-based piezoceramics

Zhongming Fan,[1,*] Shujun Zhang,[2] and Xiaoli Tan[1,*]

[1] Department of Materials Science and Engineering, Iowa State University, Ames, IA 50011, USA

[2] Institution for Superconducting and Electronic Materials, Australia Institute of Innovation Materials, University of Wollongong, Wollongong, NSW 2500, Australia

Abstract

Lead-free $(K_{0.5}Na_{0.5})NbO_3$-based (KNN) piezoceramics featuring a polymorphic phase boundary (PPB) between the orthorhombic and tetragonal phases at room temperature are reported to possess high piezoelectric properties but with inferior cycling stability, while the ceramics with a single tetragonal phase show improved cycling stability but with lower piezoelectric coefficients. In this work, electric biasing *in-situ* transmission electron microscopy (TEM) study is conducted on two KNN-based compositions, which are respectively at and off PPB. Our observations reveal the distinctive domain responses in these two ceramics under cyclic fields. The higher domain wall density in the poled KNN at PPB contributes to the high piezoelectric properties. Upon cycling, however, a new microstructure feature, "domain intersection", is directly observed in this PPB composition. In comparison, the off-PPB KNN ceramic develops large domains during poling, which experience much less extent of disruption during cycling. Our comparative study provides the basis for understanding the relation between phase composition and piezoelectric performance.

[a)]Author to whom correspondence should be addressed. Electronic mail: zfanad@iastate.edu (Z. Fan) xtan@iastate.edu (X. Tan)

1. Introduction

Ever since the milestone work by Saito et al. in 2004 [1], $(K_{0.5}Na_{0.5})NbO_3$ (KNN) has been regarded as the most promising lead-free piezoelectric ceramic. The record of piezoelectric coefficient (d_{33}) in lead-free piezoceramics kept being broken in KNN solid solutions with various chemical modifications, meanwhile the Curie Temperature (T_c) is maintained within the practicable range [2-4]. The guideline for designing new composition based on KNN is creating a polymorphic phase boundary (PPB) or morphotropic phase boundary (MPB) around room temperature, which is implemented via either decreasing the orthorhombic-tetragonal (O-T) phase transition temperature, increasing the rhombohedral-orthorhombic (R-O) temperature or forming a new rhombohedral-tetragonal (R-T) MPB [2,5]. However, the KNN composition at phase boundary has drawback: although the piezoelectric property is improved, it suffers from severe degradation upon electric cycling [6-8]. This is not very surprising because the cycling stability in other lead-free ceramics has been found sensitive to the phase composition as well [9,10]. For the device application of KNN, a compromise would have to be made by choosing the composition slightly off phase boundary so as to simultaneously guarantee both aspects.

The performance of ferroelectric materials is essentially dominated by domain response to the applied electric field. Conceivably, the KNN compositions at and off phase boundary must display distinguishable domain responses, giving rise to the different piezoelectric property and cycling stability. In this article, we conducted electric biasing *in-situ* transmission electron microscopy (TEM) to track and compare the evolution of domain morphology in two KNN-based piezoceramics. The first composition is $0.948(K_{0.5}Na_{0.5})NbO_3-0.052LiSbO_3$ (KNN−LS) which features the O-T PPB around room temperature. The other one is 2 wt% $CaTiO_3$ (~2.53 mol%) doped KNN−LS (KNN−LS−CT) with single tetragonal phase, whose O-T phase

transition temperature is shifted to below room temperature. Their ferroelectric and piezoelectric properties are listed in Table 1, extracted from the dielectric curve, P-E loop, d_{33} measurement and x-ray diffraction pattern [8,11,12]. Indeed, d_{33} in KNN−LS is ~50% higher than that in KNN−LS−CT. Upon electric cycling, KNN−LS loses nearly half of its initial polarization after 10^4 bipolar cycles. In comparison, the polarization of KNN−LS−CT remains almost unchanged [8], as shown in Fig. 1 (the P-E loops at different cycling stages can be found in Ref. 8).

2. Experiment procedures

The conventional high temperature solid-state reaction method was used to prepare the KNN−LS and KNN−LS−CT. High purity oxides and carbonates K_2CO_3 (Alfar Aesar, 99.9%), Na_2CO_3 (Alfar Aesar, 99.9%), Li_2CO_3 (Alfar Aesar, 99.9%), Nb_2O_5 (Reference Metal, 99.99%), Sb_2O_5 (Alfar Aesar, 99.99%), and $CaTiO_3$ (Alfar Aesar, 99.99%) were used as the starting materials and weighed according to the nominal compositions. After vibratory milling in anhydrous ethanol, the mixed powders were calcined at 880 °C for 2 h, and then the synthesized materials were milled again and followed by the addition of 2 wt% binder (Rhoplex). The granulated powders were pressed into pellets with 12 mm in diameter prior to the burn-out of the binder. The pellets were sintered at 1120–1180 °C in sealed alumina crucibles for 2 h.

For the *in-situ* TEM experiments on a FEI Tecnai G2-F20 microscope, as-sintered pellets were mechanically ground and polished to 120 μm thickness. Disks of 3 mm in diameter were ultrasonically cut and the center portion was thinned to 10 μm by mechanical dimpling. The dimpled disks were annealed at 450 °C for 1 hour to minimize the residual stress before Ar-ion milling until perforation. Two semicircle-shaped gold electrodes were evaporated on the flat surface of the disk with the central perforation sandwiched in between. After the specimen was

loaded on the TEM holder, thin copper wires were used to connect the electrodes to the electrical posts on the holder. Detailed configurations were explained in our previous publication [13]. During the cycling tests, bipolar cyclic electric fields in a triangular waveform of 1 Hz were applied.

3. Results

Figs. 2a and 2c show the domain morphology in KNN−LS and KNN−LS−CT at their virgin states, respectively. The two ceramics have a similar grain size but distinct domain structures. KNN−LS obviously possesses two sets of domain in the grain of interest. Even though they are both lamellar shaped and the domain walls are all on $\{110\}_{pc}$ planes (tracing along $<111>_{pc}$ directions but inclined), the domains on the right are coarser than those on the left. On the contrary, only one set of $\{110\}_{pc}$ domain wall (tracing along $<110>_{pc}$ directions but inclined) is seen in the KNN−LS−CT grain. Note that neither the orthorhombic (*Amm2*) nor the tetragonal (*P4mm*) phase in KNN features the oxygen octahedral tilting, hence no superlattice diffraction spots can help identify different phases in a grain [10]. In addition, $\{110\}_{pc}$ wall is the most common scenario in both tetragonal (90^o domain) and orthorhombic (120^o domain) ferroelectric crystals [14]. Therefore, it can be just tentatively concluded that the two sets of domain with varied domain width represent the O and T coexisting phases in KNN−LS, although it is very likely to be true owing to the room temperature O-T PPB. In comparison, the only one set of domain should represent the single tetragonal phase in KNN−LS−CT.

After the poling field is applied, the domain morphology changes dramatically in both samples. In the poled KNN−LS (Fig. 2b), the original coarse domains on the right switch to the same orientation as the left set, giving rise to an overall fine domain structure. In the poled

KNN−LS−CT (Fig. 2d), on the contrary, the major portion of the grain becomes free of domain walls. Nevertheless, it is not a perfect single domain state since some $\{110\}_{pc}$ edge-on straight domain walls (different from the original set) can still be observed close to the grain boundary. As a matter fact, a perfect single domain state is very hard to achieve since the domain walls are always needed to release the elastic energy at the grain boundary [15]. So, the poling effect in KNN−LS−CT can be described as that all the domains first switch to another equivalent orientation closer to the poling field, then they continue to coalesce into a large domain via domain walls' side-way motion [16].

Figs. 3 and 4 compare the cycling phenomena in the two compositions. The examined grain in KNN−LS contains $\{110\}_{pc}$ inclined domain walls (Fig. 3a). The absence of O/T mixed phases here might be in line with the trend that smaller grains are predominantly orthorhombic phase [14]. Under the positive poling field, the grain becomes occupied by a new set of $\{110\}_{pc}$ edge-on walls (Fig. 3c). Once the field polarity is reversed, a perpendicular set of $\{110\}_{pc}$ edge-on walls takes over (Fig. 3d). Subsequently, the bipolar cycling at ±60 V is carried out. After 100 cycles, the domain morphology has changed dramatically (Fig. 3e). Before cycling, the $\{110\}_{pc}$ walls are parallel and the domains are long. After cycling, at least three sets of domain wall are observed, nevertheless they are still on $\{110\}_{pc}$ planes, and the domains become much shorter and denser. Of particular interest is that no "domain intersection" occurs before cycling, while different sets of short domain walls are intersected with each other after cycling. To check the domain responsiveness at this stage, +60 V is re-applied. Only a few walls are mobile, while most of them are not (Fig. 3f). Of interest is that those immobile domain walls are severely intersected, forming many "rectangular" domain cells. According to the bulk cycling measurement (Fig. 1), the polarization value has dropped by ~35% after the initial 100 cycles,

while the following 9900 cycles result in ~14% decay. It infers that the *in-situ* TEM cycling test for the initial 100 cycles should be sufficient to reflect the bulk cycling behavior in KNN−LS.

On the other hand, for KNN−LS−CT, the grain of interest is viewed along $<112>_{pc}$ zone axis (Fig. 4b). The $\{110\}_{pc}$ inclined lamellar domain walls in the virgin state are tracing along a $<110>_{pc}$ direction (Fig. 4a). Under positive poling field, the major portion of the grain transforms into a large domain (Fig. 4c). Under symmetrically negative field, the residual domains near the grain boundary change their morphology but the center portion is still a large domain (Fig. 4d). It suggests that the polarization in the positive large domain state has been reversed to reach this negative large domain state. Upon bipolar cycling at ±44 V, the domain morphology changes. After 1000 cycles, some new domain walls with two different orientations form (Fig. 3e). The vertical walls trace along $[3\bar{1}1]_{pc}$ direction, and rest trace along $[\bar{1}31]_{pc}$ direction. Crystallographic analysis indicates that they are two sets of $\{110\}_{pc}$ inclined walls, but different from that in the virgin state. It should be noted that these new domain walls are distributed much sparser than the situation in cycled KNN−LS, so that many big domains remain undisrupted. As +44V is re-applied, the $[\bar{1}31]_{pc}$ tracing domain walls are mostly replaced by the vertical $[3\bar{1}1]_{pc}$ tracing walls while the relatively bigger domains are still preserved (Fig. 4f). Such a maintained responsiveness is credited to the less disrupted domain structure, especially the absence of extensive “domain intersection”, and is consistent with the stable cycling behavior in the bulk KNN−LS−CT ceramic (Fig. 1).

4. Discussion

As can be seen in Figs. 2-4, KNN−LS−CT exhibits a better domain wall mobility than KNN−LS since it reaches the large domain state more easily. Near MPB or PPB, the free energy

profile is flattened due to the co-existence of two or more ferroelectric phases, facilitating the field-induced phase transition [17]. Given the assumption that the two sets of domain in Fig. 2a representing O and T phases, the right set evolving to the same as the left set and the left set remaining unchanged (Fig. 2b) can be interpreted as the field-induced phase transition from mixed O/T phases to single T phase because the orthorhombic phase has been found not stable under electric field [18,19]. The suppressed domain wall mobility has been observed in KNN at PPB in earlier report [18], and was explained with the model proposed by Khatua et al. [20]. The model states that, the phase transition from A to B at MPB nucleates on the domain wall of phase A, which will interfere with the domain wall displacement [20]. Our observation provides a new mechanism. Any polarization arrangement other than "head-to-tail" renders a charged ferroelectric domain wall whose mobility is much suppressed compared with the neutral wall [21]. Presumably, the polarization (different direction) of O and T domains (different domain width) is difficult to form the ideal configuration, leading to a charged O/T interface that can impede the domain wall motion (Fig. 2a). Even if a grain contains only orthorhombic phase (Fig. 3a), the charged O/T interface can still form during the O→T transition (Fig. 3c). In comparison, KNN−LS−CT with single tetragonal phase is unlikely to possess charged interfaces (Fig. 2c). So, the domain wall motion could be easier, which is macroscopically manifested in the reduced coercive field (Table 1). Additionally, the harder domain switching in KNN−LS might also be partially ascribed to the greater lattice distortion within its tetragonal phase (Table 1) [22].

On top of the phase nature, the oxygen vacancy can play a critical role during, not only the poling, but also the electric cycling in piezoelectric perovskites [23]. The defect chemistry in doped KNN has been widely investigated. The acceptor doping on B-site generates oxygen vacancies or the associated defect complexes [24,25],

$$2TiO_2 \xrightarrow{KNN} V_O^{\cdot\cdot} + 2Ti'_{Nb} + 4O_O^{\times} \quad (1)$$

In the meantime, given the volatility of alkali metals,

$$O_O^{\times} + 2K_K^{\times} \xrightarrow{KNN} 2V'_K + V_O^{\cdot\cdot} + K_2O \uparrow \quad (2)$$

the donor doping on A-site can suppress the oxygen vacancies [26],

$$2CaO + 2Nb_{Nb}^{\times} + 4O_O^{\times} + V_O^{\cdot\cdot} \xrightarrow{KNN} 2Ca'_K + 2Nb_{Nb}^{\times} + 6O_O^{\times} \quad (3)$$

Combining (1) and (3) and simplify,

$$2CaTiO_3 \xrightarrow{KNN} 2Ca'_K + 2Ti'_{Nb} + 6O_O^{\times} \quad (4)$$

we can conclude that the $CaTiO_3$ co-doping is supposed to have minimal impact on the oxygen vacancies in KNN. It implies that the distinctive domain responses during poling and cycling in the two compositions can unlikely be explained by the different level of "hardening" or "domain wall pinning" effects. However, as shown in Eq. (4), the $CaTiO_3$ co-doping indeed introduces higher level of local disorder/heterogeneity [27,28], which might facilitate the initial poling towards the larger domain state in KNN−LS−CT.

So far, we have proposed the origin for the contrast in domain wall mobility despite the comparable oxygen vacancy concentration. What about the cycling stability? According to the "domain wall pinning" model, domain wall density will normally increase with the cycle number while the regular walls eventually become fragments on arbitrary planes [29]. What was observed in Figs. 3 and 4 could be the early stage of the domain fragmentation since the new sets of domain wall are still on $\{110\}_{pc}$ planes. Another possible interpretation is that the cycling in tetragonal phase won't lead to "domain fragmentation", but merely "domain intersection". It's worth noting that "domain fragmentation" was confirmed in rhombohedral phase only [29,30]. The 180° polarization switching in rhombohedral phase can be realized via multiple paths through two intermediate 60° steps. On the contrary, the situation in tetragonal phase is much

simpler because only one intermediate 90° step is needed. Consequently, "domain intersection" forms between the pinned perpendicular $\{110\}_{pc}$ walls (Fig. 3e). Once the domains are intersected, their responsiveness is considerably suppressed compared to those non-intersected ones (Fig. 3f) because the intersecting point is always charged [31].

As stated earlier, the rather stable responses under cyclic fields in KNN−LS−CT is associated with the absence of extensive "domain intersection". In the "domain wall pinning" model, domain walls and point defects are both important factors. Luo et al. has attributed the enhanced cycling stability in nonergodic $(Bi_{1/2}Na_{1/2})TiO_3$ to the absence of long-range domain walls [32]. It should be noted that the switching between positive and negative "single" domain states in KNN−LS−CT does have to go through an intermediate multi-domain state [33], of which the domain walls may also be pinned by point defects. This explains why the large domain is slightly disrupted upon cycling (Fig. 4e). However, the pinning effect due to point defects is relatively more transient than KNN−LS where dense domain walls have been permanently present after the initial poling. Therefore, KNN−LS−CT is insignificantly affected by the point defects during cycling, resulting in an improved cycling stability.

Now, we can elucidate the dilemma in KNN that we introduced at the beginning: PPB composition shows improved piezoelectric property but suffers from inferior cycling stability. Poling the KNN at PPB leaves much denser residual domain walls than poling the KNN off PPB. This implies that the extrinsic contribution might play a decisive role in the piezoelectric property in KNN, where higher domain wall density gives rise to larger extrinsic contribution of piezoelectricity [34,35]. On the other hand, the dense domain walls are nonetheless susceptible to "domain intersection" during polarization switching, leading to a rapid decay of the domain wall mobility thus decreased piezoelectric properties during cycling.

5. Conclusions

In summary, a comparative electric biasing *in-situ* TEM study is conducted on two KNN-based ceramics at and off the O-T PPB, respectively. Under poling, a large domain can readily develop in the KNN off PPB while dense domain walls preserve in the KNN at PPB. Upon cycling, the small domains become extensively intersected in the PPB composition, but the large domain is relatively resistant to disruption in the off-PPB composition. Our observations reveal that domain walls are critical to both the piezoelectric property and the cycling stability in KNN, which sheds light on the future design of KNN-based compositions ideal for the industrial applications.

ACKNOWLEDGEMENTS

This work was supported by the National Science Foundation (NSF) through Grant DMR-1465254.

[1] Y. Saito, H. Takao, T, Tani, T. Nonoyama, K. Takatori, T. Homma, T. Nagaya, M. Nakamura, Lead-free piezoceramics, Nature 432 (2004) 84.

[2] J. Wu, D. Xiao, J. Zhu, Potassium–sodium niobate lead-free piezoelectric materials: past, present, and future of phase boundaries, Chem. Rev. 115 (2015) 2559-2595.

[3] B. Wu, H. Wu, J. Wu, D. Xiao, J. Zhu, S. J. Pennycook, Giant piezoelectricity and high Curie temperature in nanostructured alkali niobate lead-free piezoceramics through phase coexistence, J. Am. Chem. Soc. 138 (2016) 15459-15464.

[4] P. Li, J. Zhai, B. Shen, S. Zhang, X. Li, F. Zhu, X. Zhang, Ultrahigh piezoelectric properties in textured (K,Na)NbO_3-based lead-free ceramics, Adv. Mater. 30 (2018) 1705171.

[5] X. Lv, J. Wu, J. Zhu, D. Xiao, X. Zhang, A new method to improve the electrical properties of KNN-based ceramics: tailoring phase fraction, J. Eur. Ceram. Soc. 38 (2018) 85-94.

[6] O. Namsar, C. Uthaisar, S. Pojprapai, Ferroelectric fatigue mechanism under bipolar electrical loading in KNN lead free piezoelectric ceramic, J. Mater. Sci.: Mater. Electron. 29 (2018) 7188-7193.

[7] F. -Z. Yao, E. A. Patterson, K. Wang, W. Jo, J. Rödel, and J. -F. Li, Enhanced bipolar fatigue resistance in $CaZrO_3$-modified $(K,Na)NbO_3$ lead-free piezoceramics, Appl. Phys. Lett. 104 (2014) 242912.

[8] S. Zhang, R. Xia, H. Hao, H. Liu, T. R. Shrout, Mitigation of thermal and fatigue behavior in $K_{0.5}Na_{0.5}NbO_3$-based lead free piezoceramics, Appl. Phys. Lett. 92, (2008) 152904.

[9] Z. Fan, J. Koruza, J. Rödel, X. Tan, An ideal amplitude window against electric fatigue in Ba TiO_3-based lead-free piezoelectric materials, Acta Mater. 151 (2018) 253-259.

[10] Z. Fan, X. Tan, A comparative study of the polarization degradation mechanisms during electric cycling in $(Bi_{1/2}Na_{1/2})TiO_3$-based relaxors, Scr. Mater. 177, (2020) accepted.

[11] S. Zhang, R. Xia, T. R. Shrout, G. Zang, J. Wang, Piezoelectric properties in perovskite $0.948(K_{0.5}Na_{0.5})NbO_3$–$0.052LiSbO_3$ lead-free ceramics, J. Appl. Phys. 100, (2006) 104108.

[12] S. Zhang, R. Xia, T. R. Shrout, Modified $(K_{0.5}Na_{0.5})NbO_3$ based lead-free piezoelectrics with broad temperature usage range, Appl. Phys. Lett. 91, (2007) 132913.

[13] X. Tan, H. He, J. -K. Shang, In situ transmission electron microscopy studies of electric-field-induced phenomena in ferroelectrics, J. Mater. Res. 20 (2005) 1641-1653.

[14] R. -P. Herber, G. A. Schneider, S. Wagner, M. J. Hoffman, Characterization of ferroelectric domains in morphotropic potassium sodium niobate with scanning probe microscopy, Appl. Phys. Lett. 90, (2007) 252905.

[15] H. Guo, C. Zhou, X. Ren, X. Tan, Unique single-domain state in a polycrystalline ferroelectric ceramic, Phys. Rev. B 89, (2014) 100104.

[16] Z. H. Zhang, X. Y. Qi, X. F. Duan, Two-step evolution mechanism of multi-domains in $BaTiO_3$ single crystal investigated by in situ transmission electron microscopy, Scr. Mater. 58, (2008) 441-444.

[17] H. Liu, S. Sun, Z. Pan, L. Fan, Y. Ren, X. Xing, J. Chen, Multiple contributions to electrostrain in high performance $PbTiO_3$−$Bi(Ni_{1/2}Hf_{1/2})O_3$ piezoceramics triggered by phase transformation, J. Eur. Ceram. Soc. 39 (2019) 5277-5284.

[18] R. Zuo, H. Qi, J. Fu, Strain effects of temperature and electric field induced phase instability in $(Na,K)(Nb,Sb)O_3$-$LiTaO_3$ lead-free ceramics, J. Eur. Ceram. Soc. 37, (2017) 2309-2313.

[19] T. Iamsasri, G. Tutuncu, C. Uthaisar, S. Wongsaenmai, S. Pojprapai, J. L. Jones, Electric field-induced phase transitions in Li-modified $Na_{0.5}K_{0.5}NbO_3$ at the polymorphic phase boundary, J. Appl. Phys. 117, (2015) 024101.

[20] D. K. Khatua, K. V. Lalitha, C. M. Fancher, J. L. Jones, R. Ranjan, Anomalous reduction in domain wall displacement at the morphotropic phase boundary of the piezoelectric alloy system $PbTiO_3$−$BiScO_3$, Phys. Rev. B 93, (2016) 104103.

[21] Z. Fan, F. Xue, G. Tutuncu, L. -Q. Chen, X. Tan, Interaction Dynamics Between Ferroelectric and Antiferroelectric Domains in a $PbZrO_3$-Based Ceramic, Phys. Rev. Appl. 11, (2019) 064050.

[22] T. Leist, T. Granzow, W. Jo, J. Rödel, Effect of tetragonal distortion on ferroelectric domain switching: a case study on La-doped $BiFeO_3$–$PbTiO_3$ ceramics, J. Appl. Phys. 108, (2010) 014103.

[23] Z. Fan, C. Zhou, X. Ren, X. Tan, Domain disruption and defect accumulation during unipolar electric fatigue in a BZT-BCT ceramic, Appl. Phys. Lett. 111, (2017) 252902.

[24] K. Kobayashi, Y. Doshida, Y. Mizuno, C. A. Randall, A Route Forwards to Narrow the Performance Gap between PZT and Lead-Free Piezoelectric Ceramic with Low Oxygen Partial Pressure Processed $(Na_{0.5}K_{0.5})NbO_3$, J. Am. Ceram. Soc. 95, (2012) 2928-2933.

[25] T. Wang, D. Wang, Y. Liao, Q. Zheng, H. Sun, K. W. Kwok, N. Jiang, W. Jie, C. Xu, D. Lin, Defect structure, ferroelectricity and piezoelectricity in Fe/Mn/Cu-doped $K_{0.5}Na_{0.5}NbO_3$ lead-free piezoelectric ceramics, J. Eur. Ceram Soc. 38 (2018) 4915-4921.

[26] S. Aggarwal, R. Ramesh, Point defect chemistry of metal oxide heterostructures, Annu. Rev. Mater. Sci. 28, (1998) 463-499.

[27] X. Sun, J. Chen, R. Yu, C. Sun, G. Liu, X. Xing, L. Qiao, $BiScO_3$ doped $(Na_{0.5}K_{0.5})NbO_3$ lead-free piezoelectric ceramics, J. Am. Ceram. Soc. 92, (2009) 130-132.

[28] F. Li, M. J. Cabral, B. Xu, Z. Cheng, E. C. Dickey, J. M. LeBeau, J. Wang, J. Luo, S. Taylor, W. Hackenberger, L. Bellaiche, Z. Xu, L. -Q. Chen, T. R. Shrout, S. Zhang, Giant piezoelectricity of Sm-doped $Pb(Mg_{1/3}Nb_{2/3})O_3$-$PbTiO_3$ single crystals, Science 364, (2019) 264-268.

[29] S. -H, Baek, C. M. Folkman, J. -W. Park, S. Lee, C. -W. Bark, T. Tybell, C. -B. Eom, The nature of polarization fatigue in $BiFeO_3$, Adv. Mater. 23, (2011) 1621-1625.

[30] H. Guo, X. Liu, J. Rödel, X. Tan, Nanofragmentation of ferroelectric domains during polarization fatigue, Adv. Funct. Mater. 25, (2015) 270-277.

[31] X. Tan, J. K. Shang, Intersection of a domains in the c-domain matrix driven by electric field in tetragonal ferroelectric crystal, J. Appl. Phys. 96, (2004) 2805-2810.

[32] Z. Luo, T. Granzow, J. Glaum, W. Jo, J. Rödel, M. Hoffman, Effect of ferroelectric long-range order on the unipolar and bipolar electric fatigue in $Bi_{1/2}Na_{1/2}TiO_3$-based lead-free piezoceramics, J. Am. Ceram. Soc. 94, (2011) 3927-3933.

[33] L. Zhang, X. Ren, Aging behavior in single-domain Mn-doped $BaTiO_3$ crystals: implication for a unified microscopic explanation of ferroelectric aging, Phys. Rev. B 73, (2006) 094121.

[34] B. Peng, Z. Yue, L. Li, Evaluation of domain wall motion during polymorphic phase transition in $(K,Na)NbO_3$-based piezoelectric ceramics by nonlinear response measurements, J. Appl. Phys. 109, (2011) 054107.

[35] D. A. Ochoa, J. E. García, R. Pérez, V. Gomis, A. Albareda, R. Rubio-Marcos, and J. F. Fernández, Extrinsic contribution and non-linear response in lead-free KNN-modified piezoceramics, J. Phys. D Appl. Phys. 42, 025402 (2008).

Table 1 Piezoelectric and ferroelectric properties in KNN−LS and KNN−LS−CT [8,11,12].

	d_{33} (pC/N)	T_{O-T} (°C)	E_c (kV/cm)	Tetragonality (c/a-1)
KNN−LS	265	35	22	1.64%
KNN−LS−CT	180	-43	18	1.46%

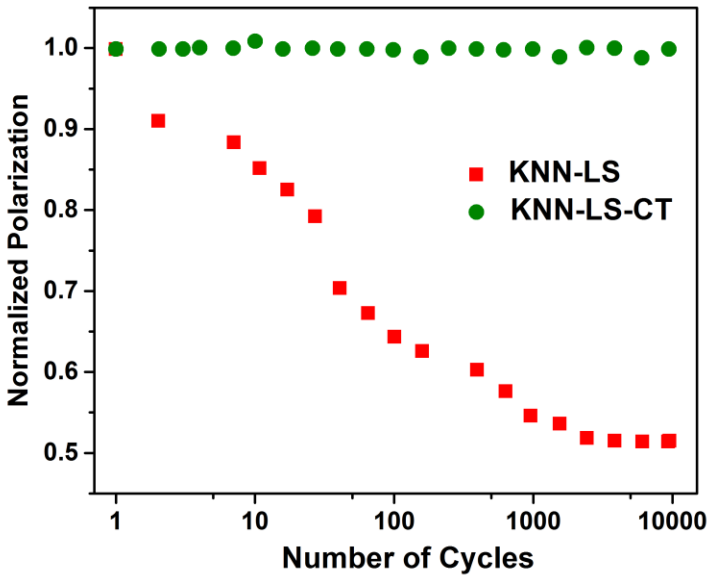

Fig. 1. Cycling stability in KNN−LS and KNN−LS−CT [8].

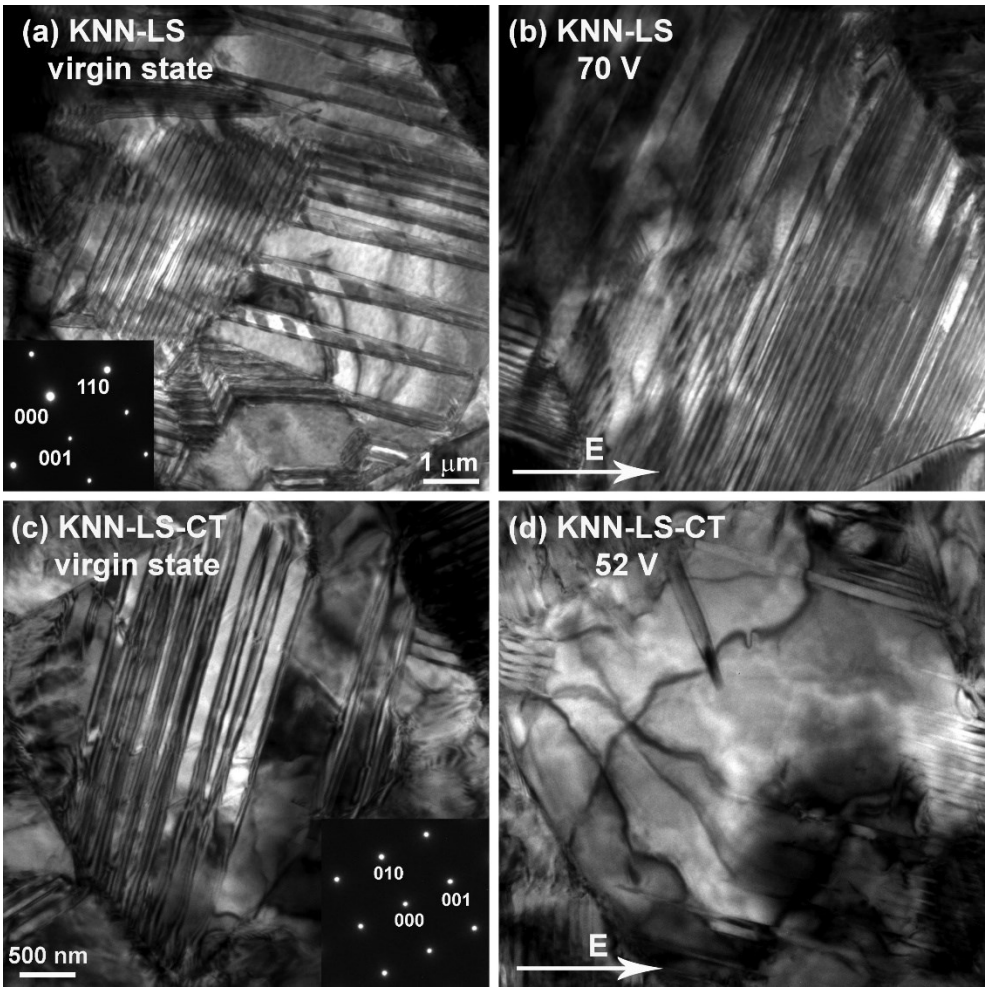

Fig. 2. The poling effect in (a)(b) KNN−LS and (c)(d) KNN−LS−CT. (a)(c) show the virgin state and (b)(d) show the poled state. The <110> and <001> zone axis electron diffraction patterns are displayed as the insets in (a) and (c), respectively. The direction of the poling field is indicated by the bright arrow in (c) and (d).

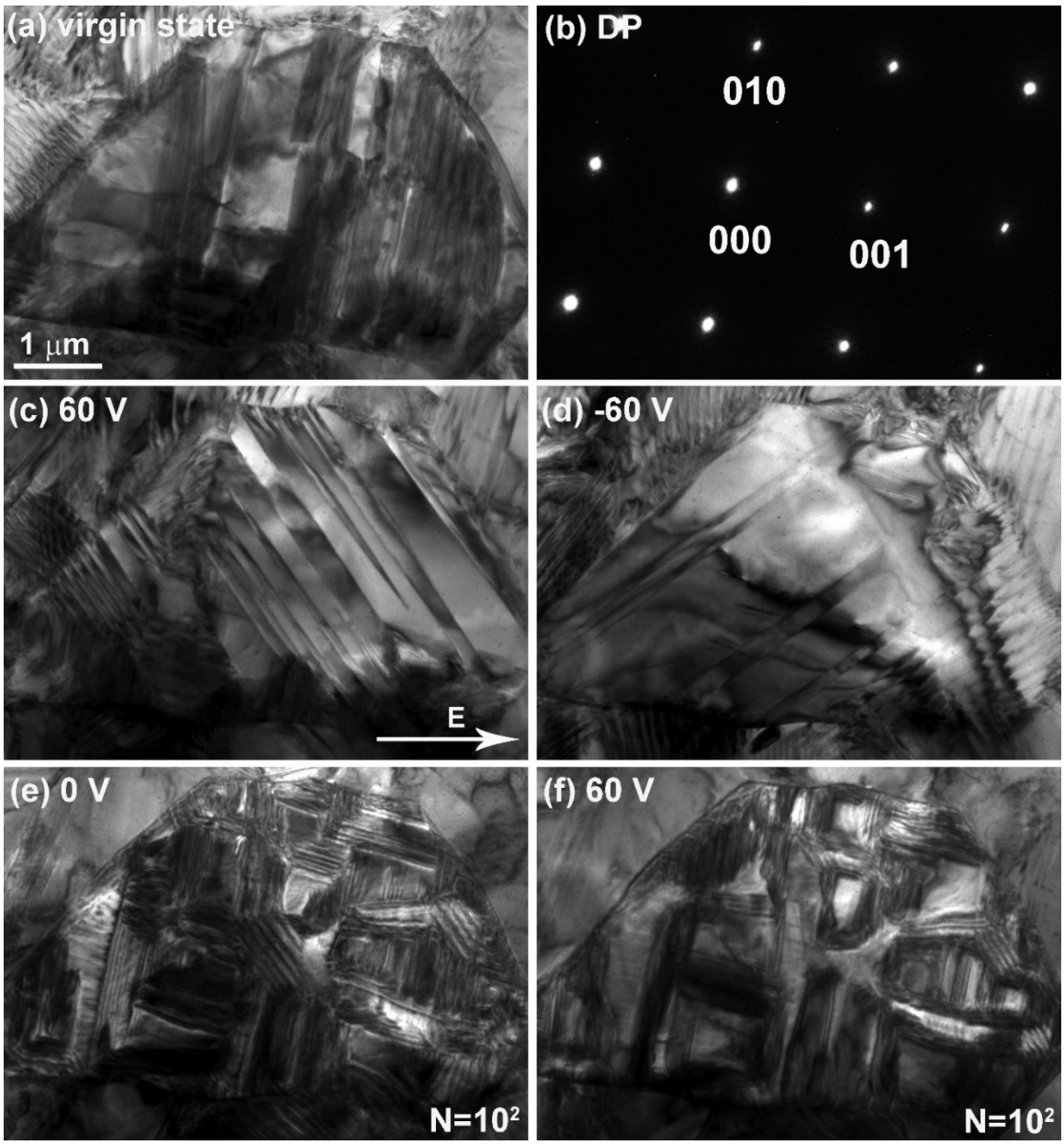

Fig. 3. (a) The virgin state in KNN−LS. (b) <001> zone axis electron diffraction pattern. (c) Domain alignment under +60 V. (d) Domain alignment under -60 V. (e) Domain morphology at 0 V after 100 bipolar cycles at ±60 V. (f) The domain responsiveness under +60 V after 100 bipolar cycles at ±60 V. The direction of the positive applied field is indicated by the bright arrow in (c).

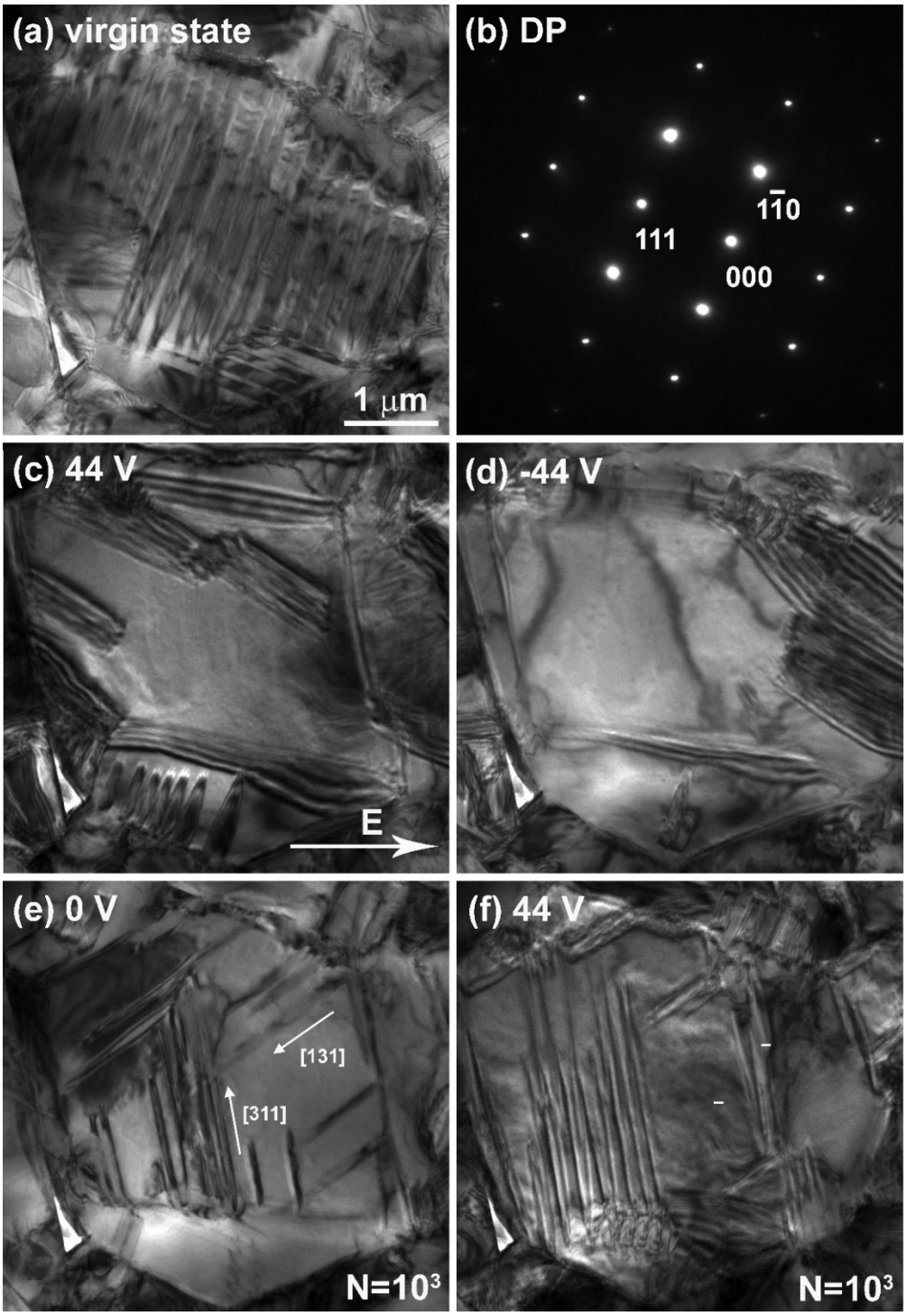

Fig. 4. (a) The virgin state in KNN−LS−CT. (b) <112> zone axis electron diffraction pattern. (c) Large domain state under +44 V. (d) Large domain state under -44 V. (e) Domain morphology at 0 V after 1000 bipolar cycles at ±44 V. (d) The domain responsiveness under +44 V after 1000 bipolar cycles at ±44 V. The direction of the positive applied field is indicated by the bright arrow in (c).